JBC RESEARCH ARTICLE

Cryo-EM structures define the electron bifurcating flavobicluster and ferredoxin binding site in an archaeal Nfn-Bfu transhydrogenase

Received for publication, October 9, 2024, and in revised form, February 13, 2025 Published, Papers in Press, March 18, 2025,
https://doi.org/10.1016/j.jbc.2025.108410

Xiansha Xiao[1], Gerrit J. Schut[2], Xiang Feng[1], Diep M. N. Nguyen[2], Haiyan Huang[2], Shuning Wang[2], Huilin Li[1,*], and Michael W. W. Adams[2,*]

From the [1]Department of Structural Biology, Van Andel Institute, Grand Rapids, Michigan, USA; [2]Department of Biochemistry and Molecular Biology, University of Georgia, Athens, Georgia, USA

Reviewed by members of the JBC Editorial Board. Edited by Joan B. Broderick

Flavin-based electron bifurcation couples exergonic and endergonic redox reactions in one enzyme complex to circumvent thermodynamic barriers and minimize free energy loss. Two unrelated enzymes designated NfnSL and NfnABC catalyze the NADPH-dependent reduction of ferredoxin and NAD. Bifurcation by NfnSL resides with a single FAD but the bifurcation mechanism of NfnABC, which represents the diverse and ubiquitous Bfu enzyme family, is completely different and largely unknown. Using cryo-EM structures of an archaeal NfnABC, we show that its bifurcation site is a flavobicluster consisting of FMN, one [4Fe-4S] and one [2Fe-2S] cluster where zinc atoms replace two additional clusters previously identified in other Bfu enzymes. NADH binds to the flavobicluster site of NfnABC and induces conformational changes that allow ferredoxin to bind between the C-terminal domains of NfnC and NfnB. Site-directed mutational analyses support the proposed mechanism that is likely conserved in all members of the Bfu enzyme family.

Electron bifurcation is the coupling of exergonic and endergonic electron transfer reaction in enzymes that minimizes free energy loss and enables thermodynamically unfavorable reactions to be catalyzed that are not dependent on ATP hydrolysis or driven by an ion gradient (1–3). Electron bifurcation was first recognized by Peter Mitchell as a key element in the ubiquinone-based Q-cycle catalyzed by Complex III of the aerobic respiratory chain (4), but it now describes a broader class of reversible enzyme reactions found in biology that oxidize an electron donor and simultaneously reduce two different electron acceptors, one of higher potential and one of lower potential (1, 5). The coupling of these redox reactions allows one of the electrons to move thermodynamically downhill, leveraging the uphill flow of the other electron. Two types of electron bifurcation are now known, one based on quinone, and one based on flavin.

Although the membrane-bound quinone-based bifurcation of the aerobic respiratory chain was discovered in the mid-70s, flavin-based bifurcation was discovered in cytoplasmic enzymes in some anaerobic microorganisms in 2008 (6, 7). These enzymes coupled oxidation of NADH (E'_0 = −320 mV, at pH 7) to reduction of the low potential electron carrier ferredoxin (E'_0 = −500 mV) with the simultaneous reduction of the more positive electron acceptor crotonyl CoA (E'_0 = −30 mV) (6, 7). Flavin adenine dinucleotide (FAD) or flavin mononucleotide (FMN) is used as the two-electron redox cofactor in flavin-based bifurcating systems that generate low-potential, high-energy compounds such as hydrogen gas (8) and reduced ferredoxin. Since 2008, many other electron-bifurcating enzyme complexes have been discovered in the cytoplasm of anaerobic bacteria and archaea (9). To date, four classes of phylogenetically unrelated electron bifurcating enzymes have been reported: 1) the electron transfer flavoprotein (EtfAB), which includes acyl-CoA dehydrogenases (*e.g.*, butyryl-CoA dehydrogenase from *Clostridium kluyveri* (7) or caffeyl-CoA reductase from *Acetobacterium woodii* (10)). These catalyze the reduction of Fd by NADH by also coupling NADH oxidation to the exergonic reduction of other small molecules, like crotonyl-CoA (7), caffeyl-CoA (11) and menaquinone (12); 2) the NADH-dependent ferredoxin NADP transhydrogenase (NfnSL from *Thermotoga maritima* (13) or *Pyrococcus furiosus* (14)), which enables NADH and Fd to be used simultaneously for the reversible reduction of $NADP^+$ for biosynthesis (Equation 1 where bifurcation is in the forward direction where Fd is a one electron acceptor/donor); 3) the methanogenic hydrogenase/heterodisulfide reductase complex MvhADG–HdrABC (*e.g.*, HdrABC-[NiFe]-hydrogenase from *Methanothermococcus thermolithotrophicus*), which uses H_2 to reduce a heterodisulfide and Fd; and 4) the BfuABC family enzymes, which include the electron bifurcating *T. maritima* FeFe- and the *Acetomicrobium mobile* NiFe-hydrogenases (15, 16). Both enzymes simultaneously and reversibly couple endergonic NADH oxidation to the exergonic oxidation of reduced Fd to generate H_2 gas. These four classes of bifurcating enzyme present a new unifying concept for energy coupling in anaerobic microbes.

$$2\ NADPH + NAD^+ + 2\ Fd_{ox} \longleftrightarrow 2\ NADP^+ + NADH + 2\ Fd_{red} + H^+ \quad (1)$$

* For correspondence: Huilin Li, Huilin.Li@vai.org; Michael W. W. Adams, adamsm@uga.edu.

Electron bifurcating flavobicluster of an Nfn transhydrogenase

The BfuABC family members are further classified into four types based on the nature of their BfuA subunits (17). In type 1 Bfu enzymes, the A subunit contains the catalytic site that reacts with third substrate of the enzyme, which feeds electrons to the BfuBC core that interacts with Fd and NAD/H. They are represented by the FeFe-HydABC hydrogenase, where its HydA contains a H_2-producing H cluster-containing domain (15), and the NfnABC, where its NfnA contains a $NADP^+$-reducing, FAD-containing domain (17). Hence NfnABC catalyzes the same reaction as the phylogenetically unrelated NfnSL (Equation 1). Type 2 and 3 Bfu family enzymes contain subunits in addition to BfuABC that feed electrons to/from the BfuA subunit, which in turn transfers them to/from the bifurcating BfuBC core. The type 2 and 3 Bfu family enzymes differ in the number and arrangement of iron sulfur clusters in their respective BfuA subunits (17). In contrast, type 4 Bfu enzymes lack BfuA but contain a BfuBC core with additional subunits. The first Bfu family member to be characterized structurally was the prototypical type 3 enzyme, the NiFe-ABCSL hydrogenase from the bacterium *A. mobile* (16), which uses two additional NiFe-hydrogenase subunits (SL, where L contains the NiFe-site) to form a bifurcating hydrogenase on the BfuABC framework. The prototypical member of the type 2 Bfu family is the tungsten-containing aldehyde-oxidizing WorABCSL (where L contains the W-pterin site), also purified from *A. mobile* (18). It should be noted that the SL subunits of these two Bfu family members (NiFe-ABCSL and WorABCSL) are unrelated to each other or to NfnSL.

The other three families of bifurcating enzymes represented by EtfAB, NfnSL, and HdrA use a single flavin, in all cases, FAD, as the sole site of electron bifurcation. This FAD accepts (donates) two mid potential electrons and transfers them individually to low and high potential pathways to reduce (oxidize) low and high potential acceptors (donors), respectively. The mechanism by which high energy low potential electrons are generated by the FAD is well understood (14). In contrast, in members of the BfuABC family, the bifurcation mechanism is noncanonical and much more complicated as their corresponding flavin, in this case, FMN, serves an electron transfer role by directly reducing the high potential acceptor (NAD) as well as being involved in electron bifurcation. From the cryo-EM structures of the *A. mobile* NiFe-ABCSL hydrogenase, bifurcation was proposed to be accomplished by the FMN in combination with a unique arrangement of four iron sulfur clusters, one in BfuC (C1) and three in BfuB (B1, B2, and B5) (17). The three subsequent structures of different FeFe-HydABC hydrogenases, from the bacteria *T. maritima* (19), *Thermoanaerobacter kivui*, and *A. woodii* (15), confirmed the cofactor arrangement within the BfuBC core, but the equivalent of the B2 FeS cluster was absent and was replaced by a zinc ion, clearly showing that the B2 site in the Bfu enzymes was not an essential part of the electron bifurcating site. Moreover, it was shown that in the *T. kivui* FeFe-enzyme, deletion of the B5 [2Fe-2S] cluster (Fig. 1*A*; termed B2 in Tki HydABC) by removing the HydB N-terminal domain (NTD) resulted in dramatic loss of

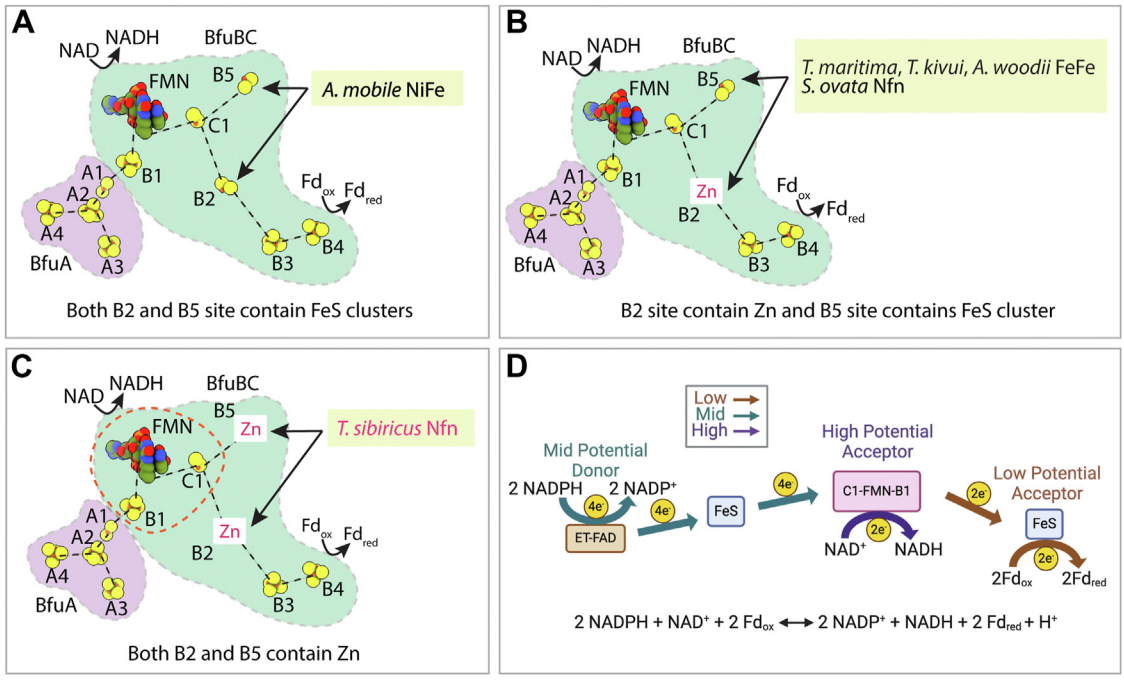

Figure 1. Current status of BfuABC family. *A*, both B2 and B5 sites contain FeS clusters in the [NiFe] hydrogenase HydABCSL from *A. mobile*. *B*, the B2 site contains Zn and the B5 site contains [2Fe-2S] cluster in the [FeFe]-hydrogenases from *Thermotoga maritima*, *Thermoanaerobacter kivui* and *Acetobacterium woodii* and the NfnABC from *Sporomusa ovata*. *C*, both B2 and B5 sites contain Zn in the NfnABC from *Thermococcus sibiricus*. *D*, schematic electron transfer pathway in the Nfn-BfuABC family of electron bifurcating enzymes in the bifurcating direction (NADPH oxidation). Fd_{ox} and Fd_{red} represent oxidized and reduced ferredoxin, respectively. *Blue arrow* indicates mid potential electron transfer pathway, *purple arrow* indicates high potential electron transfer pathway, while *brown arrow* indicates low potential electron transfer pathway. Created with BioRender.com.

bifurcation activity and that the redox state of the B5 cluster determines NADP affinity (15).

It is therefore apparent from the structures of the two different types of Bfu hydrogenase that their electron bifurcation (EB) sites consisted of FMN and three clusters, B1, B5, and C1. This was confirmed more recently by the structure of the NfnABC from the bacterium *Sporomusa ovata* (20) as this also had a zinc atom in place of the expected B2 2Fe-cluster (Fig. 1*B*). It should be noted that in the latter work this Nfn-Bfu enzyme was referred to as StnABC where its A and C subunits correspond to the C and A subunits, respectively, in the FeFe-ABC, NiFe-ABCSL, and WorABCSL enzymes. Herein for comparative purposes, we will use the nomenclature for subunits and cluster numbering as originally proposed for all members of the BfuABC family (16, 17), as shown in Figure 1, *A* and *B* (where the published *S. ovata* Stn CBA will be referred to as *S. ovata* NfnABC). In any event, all the structures of Bfu family enzymes to date are consistent with bifurcation being accomplished by a unique combination of three FeS clusters, two 2Fe- (C1 and B5) and one 4Fe- (B1), and FMN. This unit can accept a total of four electrons from the mid potential donor (NADPH or H_2) and, by a yet unknown mechanism, generate two high potential electrons as a hydride (to reduce NAD) and two individual low potential electrons (to reduce ferredoxin) according to Equation 1.

Most predicted Bfu complexes are found within the domain of Bacteria, but some are also present in the Archaeal domain of life. In particular, species of the hyperthermophilic archaeal order Thermococcaceae typically contain either an NfnABC member of the Bfu family or a member of the unrelated NfnSL family (14). Hence these two types of enzymes perform the identical metabolic function in these microbes (Equation 1), despite being completely different in terms of structure and catalytic mechanism (17). As examples, *P. furiosus* contains two versions of NfnSL (termed NfnI and NfnII (21)) but lacks NfnABC, while *Thermococcus sibiricus*, *Thermococcus kodakarensis*, and *Thermococcus litoralis* contain NfnABC but lack NfnSL. The structure of the bacterial version of NfnABC, from *S. ovata*, was recently determined (22). This confirmed the cofactor content of the bifurcation site with FMN and three clusters (C1, B1, and B5) with a Zn atom at B2 position, and that the B5 cluster plays an essential role in transferring low potential electrons ultimately to ferredoxin (22).

Herein we focus on the archaeal homolog of NfnABC from *T. sibiricus* (Tsi), which is similar to that of *S. ovata* except that the NfnA subunit in the latter enzyme is much larger by ∼200 residues (22). We determined high-resolution cryo-EM structures of Tsi NfnABC with and without bound NADH and bound Fd. We show that NADH binding triggers a series of conformational changes in Tsi NfnABC which opens a site to bind Fd. Fd binding has not been seen previously in any other member of the Bfu family. Moreover, to our great surprise, the structure provided a new definition of the electron bifurcation site in the Bfu family. The data from Tsi NfnABC show that it is comprised of FMN in close proximity to just two rather than three iron sulfur clusters, one [2Fe-2S] (C1) and one [4Fe-4S] (B1), while the third cluster, B5 [2Fe-2S], is not required, in contrast to what was recently proposed (20).

Results

Cryo-EM analysis of the purified and active Tsi Nfn-BfuABC

To elucidate the molecular mechanism of Tsi NfnABC, we expressed the Tsi NfnABC operon in the archaeon *P. furiosus*. Recombinant Tsi Nfn-Bfu was purified anaerobically *via* affinity and anion exchange chromatography steps (17). SDS-PAGE analysis demonstrated that the Tsi NfnA, NfnB, and NfnC subunits were heterologously coexpressed (Fig. S7 of reference (17)). Elemental analysis showed that Zn was the only metal other than iron present in significant amounts in the enzyme. The measured Fe:Zn ratio of 11:1 corresponds to 3.6 Zn and 40 Fe per mole. The purified enzyme exhibited electron bifurcation activity at 80 °C using NADPH to reduce added *P. furiosus* Fd but only when NAD was present (Table 1). The enzyme had very low Fd reduction activity when only NADPH was present but the rate increased 50-fold (from 0.4 to 20 units/mg) when NAD was added as the third substrate (17) (where one unit of activity is one μmole of *P furiosus* Fd reduced/min/mg). *P. furiosus* Fd is highly similar (80% identity) to Tsi Fd and both contain a single [4Fe-4S] cluster ligated by three Cys and one Asp residue. The specific activity of Tsi NfnABC (20 units/mg) is considerably lower than that (130 units/mg) previously reported for *P. furiosus* NfnSL (14). Hence the latter enzyme appears to be a more efficient system for catalyzing the reaction shown in Equation 1. We prepared the NAD(H)/Fd-bound enzyme samples by mixing purified Tsi NfnABC with NADH and/or *P. furiosus* Fd and analyzed their structures by cryo-EM. Great care was taken during the cryo-EM grid preparation procedure to prevent the exposure of the samples to air. Two-dimensional classification of the cryo-EM data clearly revealed the monomeric structural features of NfnABC enzyme (Figs. S1*C* and S2*C*).

We determined the structure of the holoenzyme form in the absence of added substrates to 2.9 Å resolution (Figs. 2*B*, S1, Table S1 and Movie S1) and to 2.8 Å resolution for the NAD(H)/Fd-bound state (Figs. 2*C*, S2, Table S1). The good resolution allowed us to build full atomic model of the NfnABC (Figs. 2*D*, S1 and S3). Interestingly, the C-terminal domain (CTD) of NfnC and the Fd domain was highly flexible and could not be modeled in the NAD(H)/Fd bound state (Figs. 2*E*, S2 and S3). The structures of the purified holoenzyme NfnABC and the NAD(H)/Fd-bound NfnABC are highly similar with an RMSD 0.19 Å for the 1435 Cα atoms shared

Table 1
Bifurcating and nonbifurcating activities of the site-directed mutants of *Thermococcus sibiricus* NfnABC

Mutation	NAD-dependent Fd reduction with NADPH (U/mg)	BV reduction with NADPH (U/mg)
WT	17.2 ± 2.4	627 ± 40
NfnA K165E (A7)	0.05 ± 0.01	224 ± 5
NfnB 4C/4A (B4)	0.76 ± 0.14	483 ± 12
NfnC ΔQ60 (linker)	6.65 ± 0.21	687 ± 44

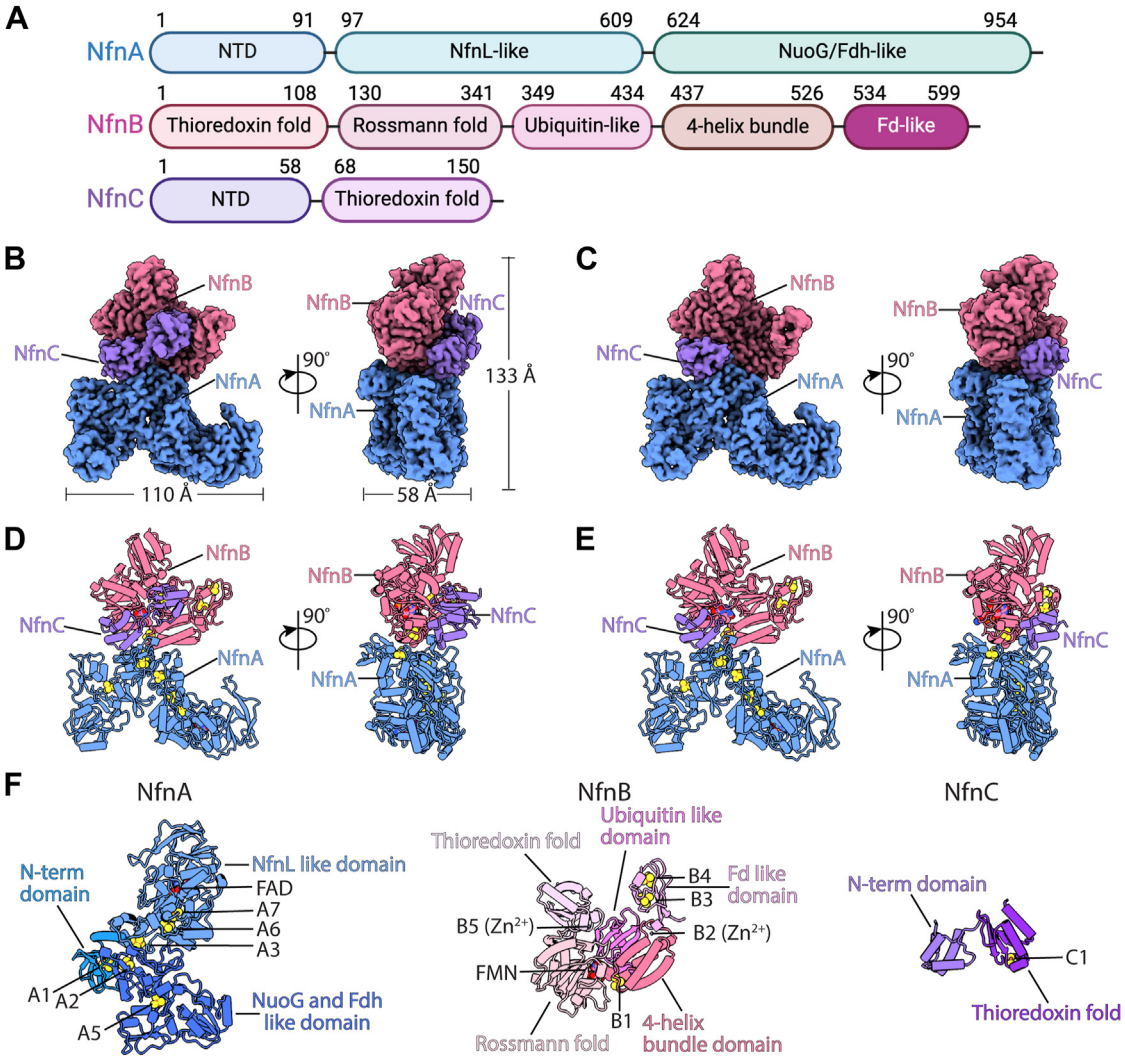

Figure 2. Cryo-EM structure of the Nfn-BfuABC from *Thermococcus sibiricus*. *A*, domain architectures of the subunits NfnA, NfnB, and NfnC. Created with BioRender.com. *B* and *C*, two orthogonal views of the cryo-EM 3D maps of the holoenzyme (*B*) and NAD(H)/Fd-bound Tsi NfnABC (*C*), segmented and colored by subunits. *D* and *E*, two orthogonal views of the structures of the holoenzyme (*D*) and NAD(H)/Fd-bound Tsi NfnABC (*E*) in cartoons. Subunits are colored as in (*B* and *C*). *F*, the domains of the individual subunits of Tsi NfnABC are shown separately with the B2 and B5 sites occupied by zinc ions.

between them, except for the above-mentioned NfnC CTD (Fig. S4).

Unlike the reported bacterial NfnABC enzyme from *S. ovata* that assembles into a D2 dodecamer composed of four heterotrimeric protomers (20), the Tsi NfnABC enzyme is a single ABC heterotrimer (Fig. 2, *D* and *E*). This observation is consistent with previous gel filtration results, which identified the enzyme as a monomeric heterotrimer (~190 kDa) (17). The heterotrimer has dimensions of 110 × 58 × 133 Å and adopts a three-lobed structure, with the NfnBC core as one lobe on top and the large subunit NfnA contributing two lobes. The NfnBC core is composed of NfnB (66 kDa and 602 aa) and NfnC (17.2 kDa and 154 aa), and the core attaches to the N terminal end of NfnA (106.8 kDa and 955 aa). The subunit interface between NfnA and NfnB, between NfnA and NfnC, and between NfnB and NfnC are 1351 $Å^2$, 532 $Å^2$, and 1703 $Å^2$, respectively, contributing to the stability of the enzyme. The NfnABC architecture resembles the other member of the Bfu family consisting of only three subunits, the FeFe-HydABC hydrogenase, except that the HydA H-cluster is absent and an FAD-containing domain homologous to the large subunit of the unrelated NfnI family of bifurcating enzymes (14) is inserted.

The mid potential electron transfer path in Tsi Nfn-BfuA

The archaeal Tsi NfnABC structure was fully resolved. Although it shares a similar architecture with the protomer of NfnABC from the bacterium *S. ovata*, Tsi NfnABC differs from Sov NfnABC by having a much shorter NfnA by 209 residues (1172 total in Sov NfnA), with an overall r.m.s.d of 1.1 Å for 476 Cα atoms (20) (Fig. S5*A*). NfnA comprises two arms that extend from the active site FAD, responsible for NADP(H) binding, to the distal [4Fe-4S] cluster (A6) (Fig. 2*F*). Tsi NfnA is highly homologous to A subunits of other members of the Bfu family for which structures are available, including the

NiFeABCSL hydrogenase from *A. mobile* (16), and the subunits of nonbifurcating enzymes such as NADH-quinone oxidoreductase from *T. thermophilus* (TthNqo3 of complex I) (23), and NAD^+-dependent formate dehydrogenases from *Rhodobacter capsulatus* (RcaFdsA of FDH) (24). Tsi NfnA lacks the long-disordered C-terminal region (83 aa) and the helix bundle close to the A6 cluster as observed in Sov NfnA (Fig. S5*A*). Instead of harboring the long loop region, the nonbifurcating Tth Nqo3 and Rca FdsA contains an extra β-barrel like domain at their C-terminal region (Fig. S5, *C* and *D*). Tsi NfnA harbors the conserved N-terminal domain (∼100 amino acids) and the NuoG/Fdh-like domains as shown by structural comparison (Fig. S5) and sequence alignment (Fig. S6). Nfn-BfuA contains three main domains as depicted in Figure 2*A* and one or more of these domains can be found in several other enzymes like; other Bfu-type complexes (such as NiFe-Bfu and FeFe-Bfu), DMSOR-like enzymes (such as FDH), the NuoG subunit of complex I, FeFe hydrogenases, and the NfnL subunit of NfnLS enzyme depicted in Figs. S3*D* and S7. This shows an extensive shuffling of these domains present in the NfnA subunit throughout the evolution of several different enzyme systems. Phylogenetic analysis revealed that the NfnL-like domain is mainly derived from the NADPH-dependent glutamate synthase but is also present in the RnfABCDGE type electron transport complex, formate dehydrogenase, FeFe hydrogenase group A, and molybdopterin-dependent oxidoreductase (Fig. S8). Notably, the NuoG/Fdh-like domain is mainly originated from the NADH-quinone oxidoreductase family (Fig. S9).

The EM map quality allowed us to identify six [4Fe-4S] clusters A1-3, A5-7, and one FAD (Figs. 2*F*, 3, *A* and *G*). These are labeled to match the NiFe-Bfu nomenclature with the A4 cluster missing and two additional [4Fe-4S] clusters (A6 and A7) from the NfnL-like domain (17). Within the edge-to-edge distance of ≤15 Å for physiological electron transfer, the chain of NfnA clusters can serve as mid potential electron transfer path in the "F-domain" of NfnA, but the A5 cluster is away from other [4Fe-4S] clusters by at least 20 Å, and this cluster is likely not involved in electron transfer in this state of the enzyme in the absence of NADH (Fig. 3*F*).

Although the overall architecture of Tsi NfnABC resembles one of the heterotrimeric protomers of NfnABC from *S. ovata* (Sov; (20)), Tsi NfnABC forms a functional heterotrimer. To understand why NfnABC does not oligomerize, we docked Tsi NfnABC to the density map of Sov NfnABC super tetramer. Notably, the interfaces of Sov NfnABC oligomers are mainly mediated by the NfnA subunit (interface 1–3) (Fig. S10*A*). In the Sov super tetramer, one protomer sits on top of another protomer mediated by the bottom long α-helix (α37) in the NuoG/Fdh-like domain of NfnA interacting with the NfnL-like domain of NfnA in another protomer (interface 1). However, in Tsi NfnABC, the corresponding α37 is rotated by 60° and is too short to interact with the NfnL-like domain (Fig. S10*B*). The other two interfaces of Sov NfnABC oligomer are mediated by the FAD-binding domain of two NfnL-like domain (interface 2), and the N-terminal NfnA domain with the NuoG/Fdh-like domain (interface 3). Tsi NfnABC lacks such extensive interactions and contains only one hydrogen bond (between Q272 and D263) and one salt bridge (between K3 and E822) at the corresponding interface −2 and −3, respectively (Fig. S10, *C* and *D*). The lack of interactions in interface 1 and the minimal interactions in interface 2 to 3 explain why Tsi NfnABC does not form a tetramer.

In the NfnA structure, FAD has well-defined density and is at the start of an electron transfer branch with only one path for electrons to transfer to the bifurcating NfnBC core (Fig. 3, *A* and *B*). Therefore, the FAD is not positioned at the juncture of two electron transfer paths for the bifurcation function. Instead, the structure of the Sov NfnABC indicates that NADPH binds adjacent to FAD to transfer electron from NADPH to the NfnA clusters (20). FAD is stabilized by hydrogen bonds with Ala-198, Asp-217, Leu-260, Trp-283, Asp-466, Ser-472, Thr-473, and Ser-477 (Fig. 3*C*) and resembles the FAD binding in the NfnL of the phylogenetically unrelated NfnSL family. However, the NfnA Arg-234 is too far (4.0 Å) to interact with the FAD N5 atom, and the N5 is instead stabilized and protects from protonation by the NfnB Arg-201 (Fig. 3*D*). The importance of R234 was verified by the mutational studies of the corresponding residue (R239) in the bacterial NfnABC (20). This observation is consistent with the distinct function of FAD, *i.e.*, electron bifurcation in the NfnSL family and electron transfer in the NfnABC family.

Among the six [4Fe-4S] clusters in Tsi NfnA, one of them (A2) is at the center of three Fe-S clusters arranged in a "Y" shape and thus at the junction of three potential electron transfer branches (Fig. 3, *E* and *F*). However, as mentioned above, A5 is 20 Å away from A2 and is unlikely to be involved in electron transfer. Because of the distances between the adjacent clusters, the A7-A6-A3 and A2-A1-B1 grouping of clusters are within electron transfer range and these merge into a single electron transfer route (A7, A6, A3, A2, A1, and B1, Fig. 3*F*). The Y-shaped constellation is found in homologous bifurcating enzymes and in some nonbifurcating complexes (25). In the previous study on the NiFeABCSL hydrogenase it was concluded that the Y-shaped constellation, or more specifically, the centrally located A2 cluster within the Y-shaped constellation, is not responsible for electron bifurcation activity (16).

Another unusual feature of Tsi NfnABC is the coordination of the A7 [4Fe-4S] cluster by three cysteines and one lysine (Lys-165) (Fig. 3*I*). From sequence analysis a similar coordination of the A7 cluster is present in archaeal NfnABC homologs, such as in *T. kodakarensis* and *T. litoralis*, but it is not an archaeal characteristic as it is also found in the NfnABC enzymes from acetogenic bacteria (22). Mutational studies of this lysine residue of the A7 cluster in Sov NfnABC to alanine or cysteine resulted in severe loss of its NADPH to methyl viologen (an artificial dye) oxidoreductase activity, whereas an arginine variant retained 50% of the WT activity, suggesting that the lysine residue is essential for efficient electron transfer (20). Interestingly, the corresponding [4Fe-4S] cluster in NfnL of the NfnSL family is coordinated by three cysteines and one glutamate residue (Fig. 3*J*), although the functional implication of this non-Cys coordination, whether to a positively (NfnA) or negatively (NfnL) charged residue, is far from clear.

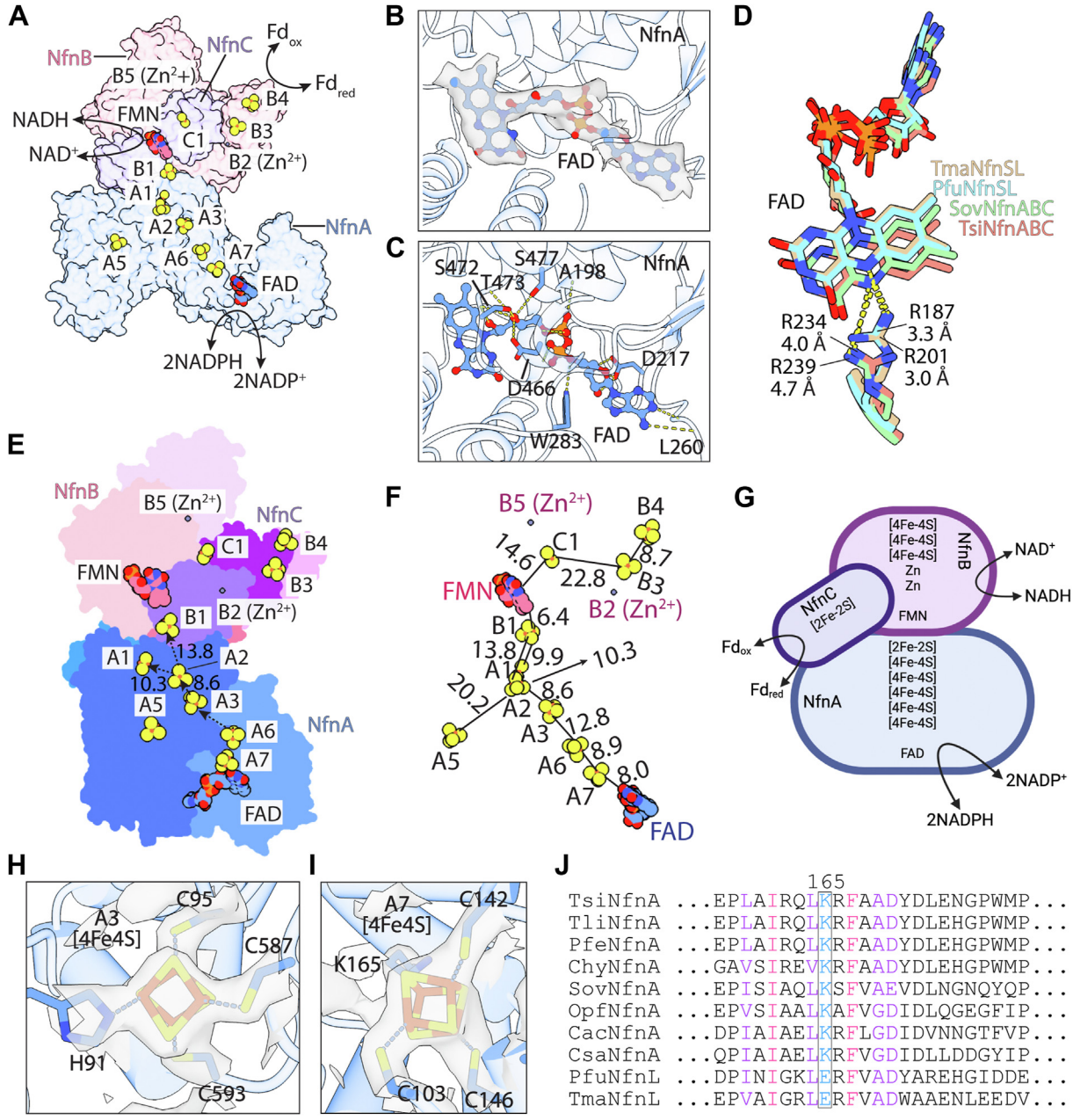

Figure 3. Cofactor organization in the Tsi NfnA subunit. *A*, overview of cofactor organization in the holoenzyme. The reduction of NAD$^+$ takes place adjacent to the FMN, and Fd is reduced at the C-terminal domain of the NfnB. *B*, close-up of the FAD binding site in Tsi NfnA, with the cryo-EM density around the FAD superimposed and shown as *transparent* surface. *C*, key residues interacting with FAD are shown in *sticks*. Hydrogen bonds between the residues and cofactors are shown as *dashed yellow lines*. *D*, superimposition of the FAD binding sites among Tsi NfnABC, Tma NfnSL, Pfu NfnSL, and Sov NfnABC. Residues R187 in Pfu NfnL and R201 in Tma NfnL form hydrogen bond with N5 of FAD, while R234 in Tsi NfnA and R239 in Sov NfnA are far from the N5 atom of the FAD. *E*, the "Y-shape" constellation of [4Fe-4S] clusters at the boundary between NfnA and NfnB in Tsi enzyme. *F*, edge-to-edge distances (Å) of the cofactors in the holoenzyme. A possible electron path is indicated by *solid lines* from the FAD in NfnA to B4 in NfnB. In this structure, the distance between C1 and B3 cluster is beyond electron transfer. *G*, subunit organization of the Tsi NfnABC enzyme and their associated cofactors. Created with BioRender.com. *H* and *I*, close-up of the A3 and A7 [4Fe-4S] clusters in NfnA superimposed with their EM densities. *J*, sequence alignment of the [4Fe-4S] A7 coordinating residues in Tsi NfnA homologues. *Pink* represents identical residues, *blue* indicates the conserved lysine coordinating with the A7 cluster, and other colors represent conserved residues.

The cofactor content of the NfnBC core is unique among Bfu family members

Like many NADH-quinone oxidoreductases (TthNqo1) (23), NAD$^+$-dependent formate dehydrogenases (RcaFdsB) (24) and the NAD$^+$-reducing [NiFe] (AmoHydB) (16) and [FeFe] hydrogenases (AwoHydB and TkiHydB) (15), the Tsi NfnB contains a Rossmann-like fold (residues 117–331), a ubiquitin-like domain (residues 332–425), and a 4-helix bundle (residues 426–526) (Figs. 2*F*, S7, S11 and S12). The Rossmann-like fold contains the conserved binding site for the electron acceptor NAD$^+$ and the electron bifurcating FMN. The B1 [4Fe–4S] cluster in Tsi NfnB is coordinated between the Rossmann-like fold and the 4-helix bundle (Fig. 2*F*). However, in contrast to the B subunit in the NiFe-ABSCL

hydrogenase, Tsi NfnB contains a Zn^{2+} at the B2 position in the linker region between the NfnBC core and the CTD, similar to what was found in the acetogenic bacterial NfnABC (20) and in the three FeFe-ABC hydrogenases (15, 19). In contrast to the NiFeABCSL enzyme, where its B2 [2Fe-2S] cluster has His/Cys penta-coordination (16), the Zn^{2+} ion in the B2 position in Tsi NfnB is tetra-coordinated by three Cys (C437, C529, and C534) and one His (H524) (Fig. 4*A*). The additional Cys coordinated in the NiFe-enzyme (C476) replaced by Thr in NfnB, as it is in the acetogenic bacterial NfnB and in the FeFe-ABC hydrogenases from *T. kivui* and *T. maritima* (15, 17) (Fig. S11). H524 in Tsi NfnB is conserved in virtually all B subunits of the Bfu family, but is not present in HydB homologs (17). The Fd-like domain contains two [4Fe–4S] clusters (B3 and B4), is loosely attached at the outer edge of the NfnBC core. The NfnB linking hinge between the Fd-like domain and the four-helix bundle domain bears a Zn^{2+} (B2) rather than an Fe-S cluster (Figs. 4*A*, S13*B*), similar to the Nfn-type BfuB from *S. ovata* (20) and the [FeFe] hydrogenases (AwoHydB and TkiHydB) (15) (Figs. S12 and S13*A*). The two [4Fe-4S] clusters B3 and B4 are each ligated by four cysteines which are part of the two conserved ferredoxin signature motifs CX2CX2CX3CP (11). Like all BfuC subunits in the bifurcating Bfu family, Tsi NfnC consists of an N-terminal 4-helix bundle (aa 3–64) and a C-terminal thioredoxin-like domain (aa 65–150) (Figs. 2*F*, S7 and S14). The NfnC thioredoxin-like domain is structurally similar to the N-terminal thioredoxin-like domain of NfnB but contains a spinach

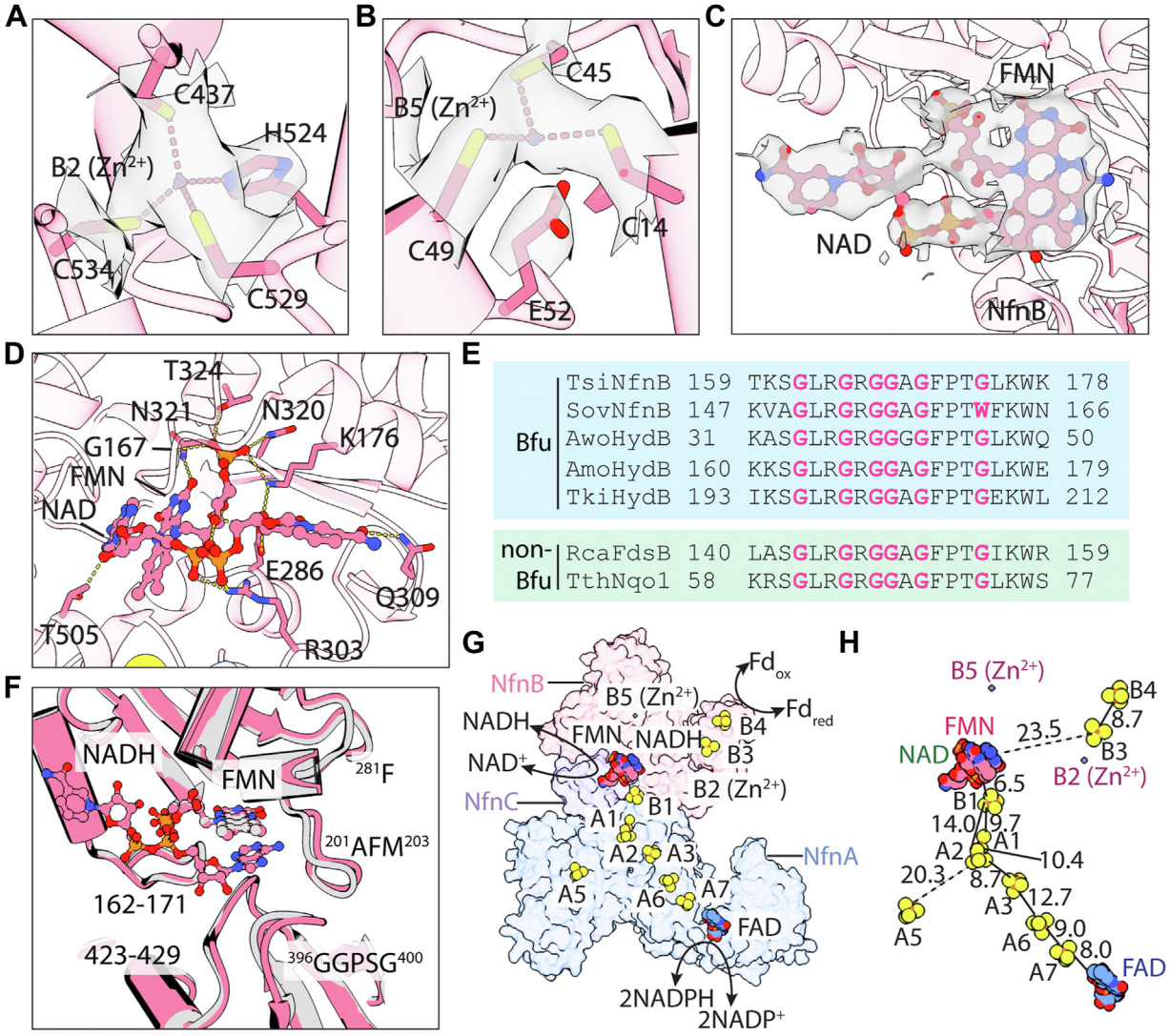

Figure 4. Cofactor coordination in the bifurcating Tsi NfnBC core. *A* and *B*, close-up view of the two Zn binding site in NfnB superimposed with the EM densities in transparent surface view. *C*, close-up view of the NAD^+/FMN binding site in NfnB superimposed their EM density in transparent surface view. *D*, key residues interacting with NAD^+ and FMN are shown in *sticks*. Hydrogen bonds between the residues and cofactors are shown as *dashed yellow lines*. *E*, sequence alignment of the NAD^+/FMN coordinating residues of the Tsi NfnB homologues. The conserved glycine residues are in *pink*. *F*, key NfnB loops coordinating FMN and NADH. These loops in FMN-bound state are superimposed with NAD(H)/Fd bound state to show conformation changes. The starting and end residues numbers of the five coordinating loops are labeled. *G*, overview of cofactor organization of NAD(H)/Fd-bound NfnABC, highlighting the NAD^+/FMN site, the FAD site, the Zn sites, and the [4Fe-4S] site. Note that the CTD of NfnC is highly flexible and is not modeled in the NAD(H)/Fd-bound enzyme. *H*, edge-to-edge distances (Å) of the cofactors in the NAD(H)/Fd-bound NfnABC structure. CTD, C-terminal domain.

ferredoxin-like [2Fe-2S] cluster (26). The C1 [2Fe-2S] cluster is coordinated by C74, C79, C115, and C119 in a hydrophobic environment close to the surface.

The most striking feature of the Tsi NfnBC core is the B5 site (Figs. 1 and 4*B*) which has been shown to be a [2Fe-2S] cluster in all of the structural models of Bfu family members so far, including the NiFe-ABCSL hydrogenase (16), the three FeFe-ABC hydrogenases (15, 19), and the Sov NfnABC (20) (Figs. S12 and S13*C*). However, in Tsi NfnB the B5 site is unequivocally resolved as a Zn^{2+} ion (Figs. S12*A* and S13*D*). Attempts to model a [2Fe-2S] cluster at this site resulted in steric clashes with the coordinating Cys residues (Fig. S13*E*). This gives a completely new perspective on the nature of the electron bifurcating site in the archaeal Nfn as it must consist, not of FMN and three clusters (B1, B5, and C1) that are present in all known BfuB structures as previously proposed (17), but of a flavobicluster containing FMN and the B1 and C1 clusters (Fig. 1). Clearly, redox inactive zinc at the B5 site is present in an active electron bifurcating Nfn enzyme and cannot be involved in electron transfer, in contrast to the B5 [2Fe-2S] cluster in the FeFe-ABC hydrogenase that was shown through mutagenesis studies to be essential to bifurcation activity (15). Hence the unique flavobicluster EB site is simpler than previously assumed consisting of FMN and two iron–sulfur clusters, and we propose that this same site is used, not just in Tsi NfnABC, but in all members of the Bfu family (17).

The flavobicluster bifurcation site in the NfnBC core

The FMN in Tsi NfnB is bound by a network of interactions in an extended, solvent-accessible cavity with a glycine-rich loop (Fig. 4*C*). The isoalloxazine ring of FMN is within 15 Å of the B1 and C1 iron–sulfur clusters, with the C8-methyl of the dimethylbenzene moiety of the flavin pointing toward the B1 [4Fe-4S] cluster (6.4 Å), the N5-containing edge facing the C1 [2Fe-2S] cluster (14.6 Å), and the ribityl phosphate tail extending away from both iron–sulfur clusters (Figs. 3*F*, 4, *G* and *H*). The FMN binding pocket also accommodates the NAD(H) substrate (Fig. 4, *C*–*F*). The nicotinamide ring of NADH is inserted deep into the binding pocket and stacks against the flavin ring of FMN. The β-phosphate of NADH is held in place by a salt bridge with NfnB Arg-303 and two hydrogen bonds with the O2′ and O4′ hydroxyl groups of FMN's ribityl moiety (Fig. 4*D*). The adenosine base of NADH resides in a hydrophobic pocket, but the adenosine O2′ hydroxyl and O3′ hydroxyl are within hydrogen bond distance with the carboxyl group of Glu-286. This places a negative charge adjacent to the O2′, ensuring selectivity of NfnB for NADH over NADPH (27). Five signature motifs surround the FMN and NAD-binding pocket: loop 162 to 171, the Ala-Phe-Met (AFM) motif (aa 201–203), the Phe-281 in loop 278 to 287, the GGPSG motif (aa 396–400), and loop 423 to 429 (Fig. 4*F*). The GGPSG loop is highly conserved in all bifurcating enzymes as shown by the sequence alignment (Fig. S11). These residues (A201, M203, and F281 in Tsi NfnABC) are highly conserved in the FMN- and NADH-binding domains of Tsi NfnB in the BfuABC family of enzymes and are absent in nonbifurcating enzymes (Fig. S11) (17). Unlike the bifurcating NfnSL family of enzymes that have an Arg or Lys in the vicinity of the isoalloxazine ring of the bifurcating flavin to stabilize a fully reduced flavin state, the BfuABC family of enzymes and the nonbifurcating flavin in the NfnSL family lack a positively charged residue next to FMN but have a negatively charged Asp-195 to stabilize a flavo-semiquinone state instead (Fig. S15).

Thus, the Tsi NfnABC structure coordinates a network of adequately spaced [4Fe-4S]-clusters that connects these clusters to the bifurcating flavobicluster in the NfnBC core (Fig. 4, *G* and *H*). FMN sits at the end of the mid potential electron transfer path composed of FAD-A7-A6-A3-A2-A1-B1. The electron donor NADPH is expected to bind next to the FAD (20), and electrons are transferred *via* the five [4Fe-4S] clusters in NfnA to the B1 [4Fe-4S] cluster in NfnB adjacent to FMN. The unique flavobicluster site of B1-FMN-C1 bifurcates the incoming electrons by an unknown mechanism to reduce the high potential acceptor NAD and to reduce Fd *via* a low potential path involving C1, B3, B4, and Fd (Figs. 1*E*, 4*H*, 5*A*). The B5 site (and B2 in the case of the NiFe-enzyme), which was proposed to play a role in electron transfer in other Bfu enzymes, is not involved in Tsi NfnABC. In the EB site in the holoenzyme without added NADH/Fd, the C1 [2Fe-2S] cluster is 14.6 Å from the FMN, barely close enough for electron transfer, and 22.8 Å distant from the B3 cluster, too far for electron transfer to occur. Therefore, the resting enzyme conformation has no pathway for low potential electron transfer to Fd, and a large conformational change in the enzyme structure is anticipated to complete the electron transfer in this branch of electron bifurcation process.

The NfnC CTD movement gates electron bifurcation

As mentioned above, the EM density of the NfnC CTD containing the C1 cluster is well-defined in the holoenzyme, but this density becomes poorly defined in the NADH-bound state, suggesting that NAD binding may have enabled the NfnC CTD to exist in multiple conformations. Therefore, we performed a 3D variability analysis (3DVA) (28) and isolated three 3D classes showing variation of the NfnC CTD containing the C1 [2Fe-2S] cluster with respect to the B3 and B4 [4Fe-4S] clusters in NfnB (Fig. 5 and Movie S2). We presume the three 3D classes represent three major solution states, although more states must coexist given the high dynamics of the NfnC CTD. In the first state (conformer 1), the NfnC thioredoxin-like CTD binds to the NfnB core domain tightly in a closed conformation (NfnC-CTD-in) (Fig. 5*A*-i-ii). The distance between the C1 cluster and FMN is 14.2 Å, within the electron transferring 14 Å distance. So, the C1 cluster in this state is participating in electron bifurcation in combination with B1 and FMN (Fig. 5*A*-iii). We refer to this state as the electron bifurcation state or B-state.

In the second state (conformer 2), the NfnC CTD rotates 45° toward the NfnB Fd-like domain. In this "NfnC-CTD-out" state, the C1 cluster is now 10.4 Å from the B3 and B4 clusters, much closer than the 21.8 Å distance in the first and "NfnC-

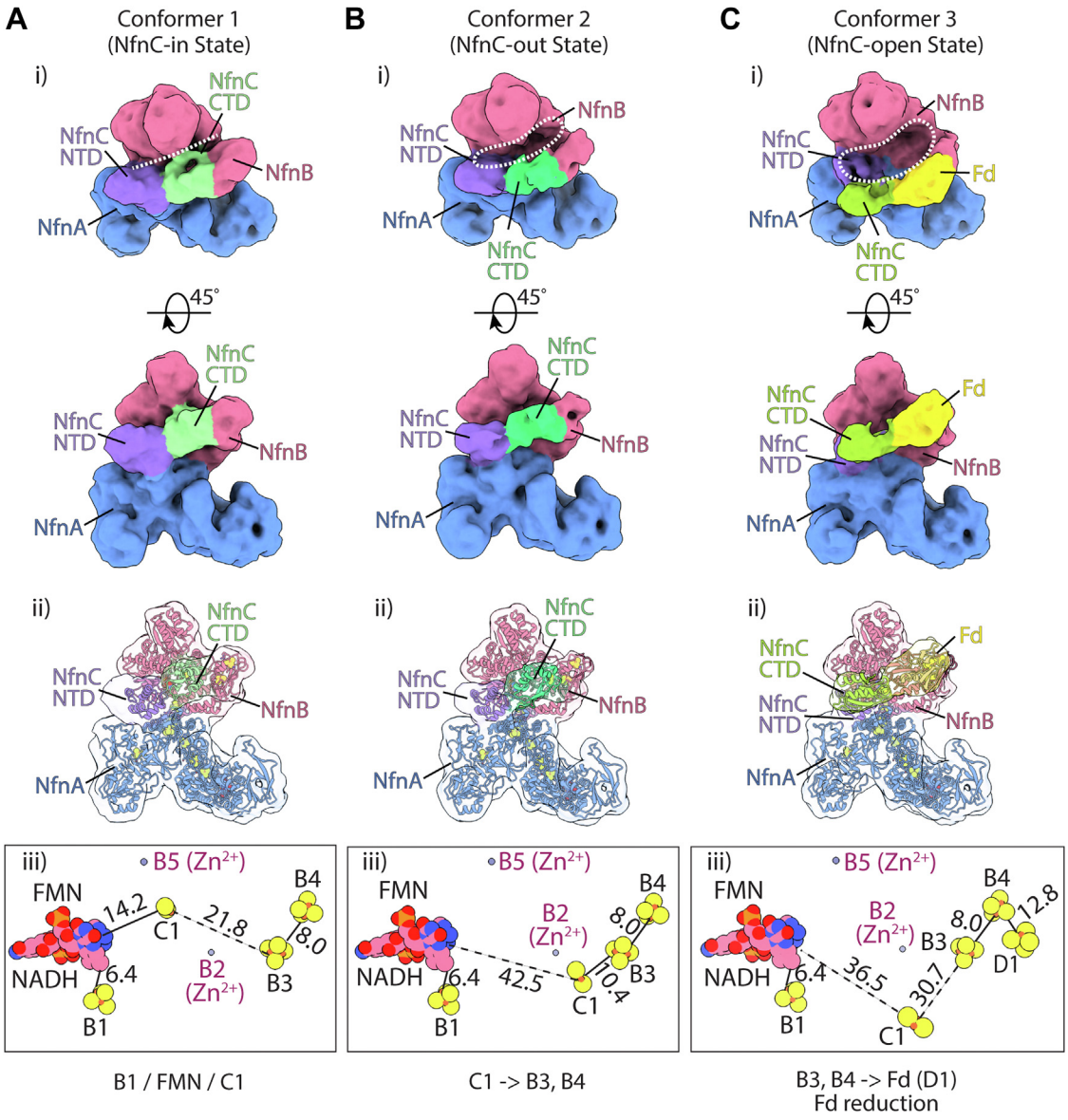

Figure 5. Three 3D Variability Analysis-derived conformations of the Tsi NfnABC enzyme in the presence of NADH and Fd. 3D models were generated using 3D variability analysis with particles low pass filtered to 8 Å. EM 3D maps (i) are colored by proximity to the subunit indicated as modeled using rigid body fitting (ii). *A*, in the NfnC-in state (conformer 1), NfnC CTD locates in between the NfnC NTD and the NfnB Fd-like domain, where C1 is close to FMN but far from B3/B4 (A-iii). *B*, in the NfnC-out state (conformer 2), NfnC CTD moves outward to a position between NfnC NTD and NfnB Fd-like domain, making C1 close to both B3 and B4 but farther away from FMN (*B*-iii). *C*, in the NfnC-open state (conformer 3), NfnC CTD moves outward which leaves space for Fd binding in between the NfnC CTD and the NfnB Fd-like domain. The *dashed white shape* highlights the gap size between NfnB and NfnC. The distance between B3/B4 to D1 is 12.8 Å (*C*-iii). CTD, C-terminal domain; NTD, N-terminal domain.

CTD-in" state (Fig. 5*B*-i-ii), and the C1 to FMN distance is further extended to 42.5 Å (Fig. 5*B*-iii). Large conformational changes involving the CTD of NfnC and the Fd-like domain of NfnB have also been reported in other Bfu family members, including the NiFeABCSL (16) and FeFeABC hydrogenases (15). In the NiFeABCSL enzyme, the HydC subunit CTD rotates by 24° and tilts toward the B3 and B4 clusters, shortening the C1 to B3 distance to 13.4 Å for electron transfer, while in the FeFe-enzyme, the CTD rotates outward to shorten the distance from the C1 to B3 and B4 clusters to 15 to 18 Å. Further, a kinetic simulation of the FeFe-ABC also supported electron transfer from the C1 to the B3 and B4 clusters in the HydC-out conformation.

In the third state (conformer 3), the NfnC CTD rotates ~90° outward to form an open conformation (NfnC-CTD-open) (Fig. 5*C*-i-ii). The NfnC CTD contact with the NfnB ubiquitin-like domain is lost, and instead a new density appears between these two domains. We added Fd to the enzyme. Focused 3D classification and refinement revealed a well-defined EM density that fits well as a rigid body with atomic model (Protein Data Bank ID 3SIZ) (Fig. S16, *A* and *B*). Hence, we have assigned the new density as Fd. This is the first experimental data from any Bfu enzyme that demonstrates where Fd binds since in all previous Bfu structures Fd was only computationally modeled (15, 16, 20). Moreover, in these models, Fd was predicted to bind near the terminal B4 cluster

in the NfnB Fd-like domain, where low potential electrons transfer directly from B3 to B4 to Fd. However, as we show here in Tsi NfnABC, Fd binds in an unprecedented position compared to what has been previously proposed. Specifically, in Tsi NfnBC, in the rigid-body docked pose, the single [4Fe-4S] cluster (D1) of Fd is 12.8 Å from both the B3 and the B4 cluster in the NfnB Fd-like domain and is 28.7 Å from the C1 cluster (Fig. 5*C*-iii). In this "NfnC-CTD-open" state, the C1 to B3/B4 distance is over 30 Å, which allows forward electron transfer from the B3 and B4 clusters to reduce Fd but prevents electron from flowing backwards. Thus, this state is ready for Fd reduction.

Hypothetical electron bifurcation mechanism in Tsi NfnABC

Our structural analysis has revealed that the Tsi NfnABC is relatively rigid in resting state in the absence of any substrate but becomes highly dynamic and undergoes large conformational changes upon NAD and/or Fd binding. These observed conformational changes are likely redox driven during catalysis and are associated with electron transfer process during the bifurcation reaction. We therefore propose a conformation-change coupled multi-step electron transfer process (Fig. 6). The reaction cycle is initiated by NADPH binding to NfnA and donating two mid potential electrons to FAD (Fig. 6*A*). Electrons are then transferred *via* the mid potential route formed by the clusters in NfnA to reach the NfnBC core containing the flavobicluster bifurcation site of FMN with adjacent B1 and C1 clusters. Reduction of FMN generates a one-electron reduced semiquinone state, which is likely stabilized by Asp-195. The bifurcation reaction by the flavobicluster site is probably governed by the NAD binding adjacent to FMN in NfnB, which induces the first major conformational change in the NfnBC core to bring the C1 cluster within electron transfer range of the FMN. In essence, NAD binding in and of itself generates this flavobicluster EB site so that electron bifurcation can occur – which is observed in the "NfnC-CTD-in" state (conformer 1) (Fig. 6*B*).

The distances between FMN and C1 (14.2 Å) in the "NfnC-CTD-in" state is within the electron transfer range, suggesting a bifurcation (BF)-competent state. The reduction of the C1

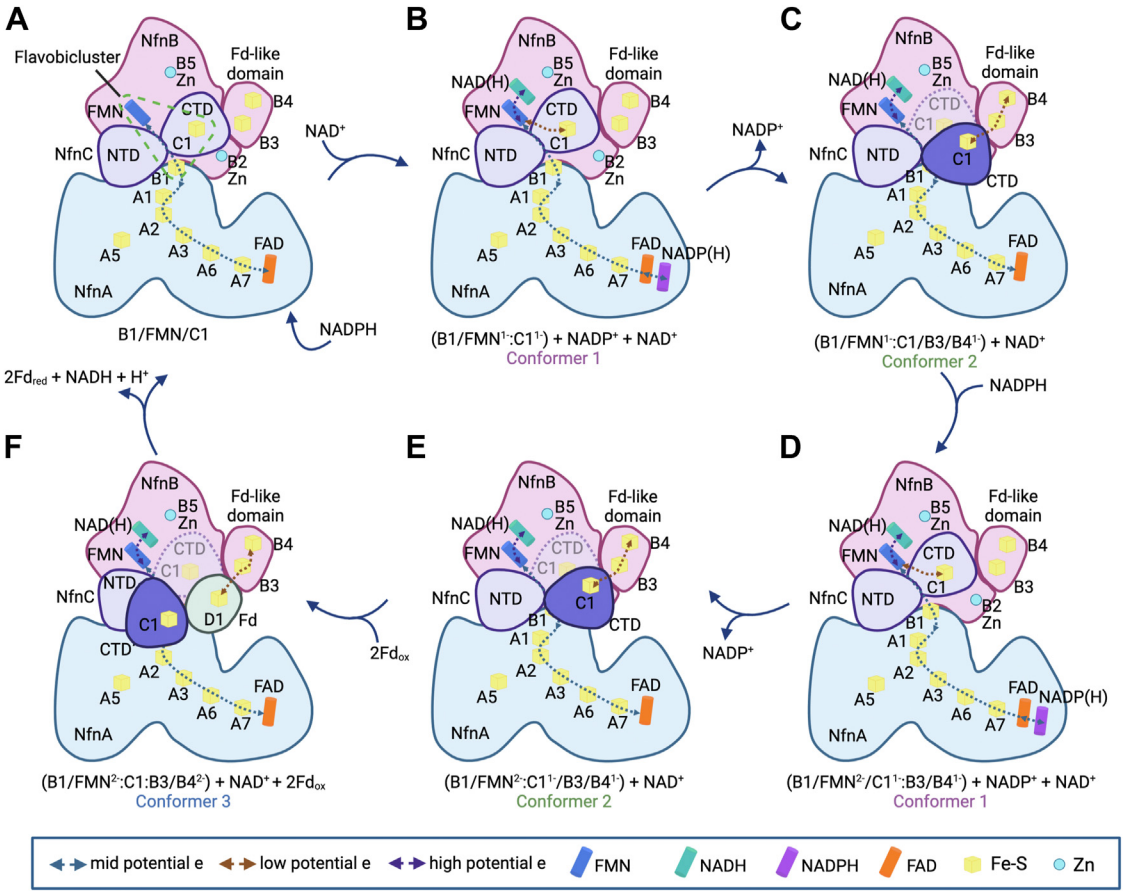

Figure 6. Putative electron bifurcation mechanism of the Tsi NfnABC enzyme. Binding and oxidation of NADPH initiate the reaction in NfnA. For the first round of NADPH oxidation, electrons travel along the [4Fe-4S]-clusters in NfnA (A7-A6-A3-A2-A1) to the electron bifurcation site consisting of B1-FMN-C1 (*A*). NAD binding adjacent to FMN in NfnB induces the first major conformational change in the NfnBC core (conformer 1) to bring the C1 cluster within electron transfer range of the FMN (*B*). The B1-FMN-C1 flavobicluster site donates two electrons as a hydride to the high potential acceptor NAD^+, which also accepts electrons from the mid potential pathway formed by the [FeS] clusters in NfnA and transfers them *via* the C1 cluster to the B3/B4 clusters, the low potential acceptor, *via* the second major conformational change (conformer 2) (*C*). The second round of NADPH oxidation leads to a series of conformational switches between conformer 2 and conformer 1 allows C1 accept the second round of electrons from FMN (*D*) and transfer to the B3/B4 cluster (*E*). Subsequently, the third large redox-driven conformational change (conformer 3) leads to Fd binding and the low-potential electron transfer from the B3/B4 clusters to Fd (*F*). With the release of Fd, a new cycle starts. Panels were created with BioRender.com.

cluster was suggested to increase the affinity for $NAD(P)^+$ in the HydBC core in [FeFe] hydrogenase (15). The dissociation of oxidized $NADP^+$ triggers a conformational change from the NfnC-CTD-in to the NfnC-CTD-out state, as observed in the conformer 2 structure, which allows efficient electron transfer from C1 to B3 (Fig. 6*C*). The electrons reside within the B3/B4 clusters. Binding of the second molecule of NADPH triggers the conformational switching back to the NfnC-CTD-in state, which initiates a new reaction cycle upon further electron transfer from the mid potential pathway formed by the iron–sulfur clusters in NfnA (Fig. 6, *D* and *E*). The bound NAD^+ increases the redox potential of the flavin, which leads to a complete two-electron reduction of FMN to the $FMNH^-$ form upon the second NADPH oxidation step. The $FMNH^-$ state further triggers a proton-coupled electron transfer to yield NADH. Once C1 accepts a new round of electrons and transfers to B3/B4, electrons residing within the B3/B4 module favor the thermodynamically uphill reduction of the low potential acceptor Fd (Fig. 6*F*) and prevents electron back transfer to the flavin module. This is different from the role of the BF-FAD in the FBEB enzyme systems, but how the FMN-based flavobicluster achieves bifurcation is not clear based on the current knowledge of flavin chemistry.

A series of redox-driven conformational changes leads to Fd binding but, unexpectedly, this takes place between NfnC-CTD and the NfnB Fd-like domain, which contains the B3/B4 clusters (Figs. 5*C* and 6*E*). Hence, in the Fd bound conformation, the D1 [4Fe-4S] cluster of Fd is within 13 Å of both B3 and B4 clusters and direct electron transfer is possible, while C1 is more than 30 Å from the Fd D1 cluster, which blocks reverse electron transfer. Similar redox-driven conformation-change coupled low potential electron transfer to Fd has also been proposed to occur, based on modeling the Fd, in the Bfu family members FeFe-ABC and NiFe-ABCSL hydrogenases (15, 16) and in the Sov NfnABC (20), which all propose direct electron transfer of low potential electrons from B3/B4 to Fd. However, all of these involve the direct interaction of Fd solely with the NfnB Fd-like domain, which differs from the Tsi NfnABC structure resolved in this work, where we demonstrate that the Fd is wedged between the NfnC-CTD and NfnB Fd-like domain but positioned closer to NfnB Fd-like domain. We would suggest that the latter is a conserved general feature of electron bifurcation in this family of enzymes.

Probes of the structure/function of NfnABC by site-directed mutagenesis

Site-directed mutations were made at each of the three subunits of NfnABC to provide some insight into the proposed mechanism based on the determined structure. Specifically, the NfnA K165E, the NfnB 4C/4A and the NfnC ΔQ60 and ΔFRFEP (linker) mutants were constructed to investigate, respectively, the role of the Lys residue coordinating the A7 cluster by mutation to Glu, the role of the B4 cluster by total replacement of its four coordinating Cys residues by Ala, and the role of the 11-residue linker (Y58-AQFRFEPLG-K68) that serves to link the CTD and NTD of NfnC, the relative movement of which is proposed to be critical for the electron bifurcation reaction. In the latter case, the linker was reduced to either 10 (ΔQ60) or 6 (ΔFRFEP) residues. Of the four mutant enzymes, three were successfully purified by affinity (His-) and anion exchange (QHP) chromatography (Fig. S17).

In NfnA, the A7 [4Fe-4S] cluster is the closest redox cofactor to the nonbifurcating FAD of NfnA (Fig. 3*A*). This cluster is distinguished by replacement of the expected C165 by Lys, a replacement conserved in all NfnABC enzymes (Figs. 3, *I* and *J*, S18). Herein, we constructed the mutant K165E of NfnA and this resulted in almost complete loss of bifurcation activity, coupling NADPH oxidation to the simultaneous reduction of Fd and NAD, but, unexpectedly, about one third of the nonbifurcating activity coupling NADPH oxidation to artificial dye (benzyl viologen, BV) reduction remained (Table 1). This gives a different perspective on the mechanism of bifurcation since the A7 [4Fe-4S] cluster is remote from the proposed flavobicluster BF-site of FMN/C1/B1 and still supports high NADPH oxidation activity, yet bifurcation does not occur. Kumar *et al.* (2023) (20) found that when the corresponding Lys residue in the Sov NfnABC enzyme was mutated to Arg, approximately 50% of the bifurcating activity was lost, but all of the activity was lost in the Lys to Cys mutant. Interestingly, the [4Fe-4S] cluster adjacent to the bifurcating FAD in the NfnL subunit of the unrelated NfnSL also has one of the expected Cys replaced, this case by Glu (21). As shown in Fig. S18, the 14-residue region surrounding this position (Lys in NfnA and Glu in NfnL) is highly homologous between these otherwise unrelated enzymes. Hence, non-Cys ligation to key iron sulfur clusters is clearly a critical aspect to BF-reactions in general.

The structure of Tsi NfnABC shows that there is a 11-amino-acid-residue-long linker (Y58-K68) between the CTD of NfnC, which contains the C1 [2Fe-2S] cluster, and its NTD (Fig. 2, *A* and *F*). As discussed above, during bifurcation the CTD moves away from the FMN toward the B3 and B4 clusters thereby preventing short-circuiting of the low potential electrons. As shown in Fig. S19, the two domains are tethered by a highly conserved linker between helix α4 and sheet β1 of NfnC. To impede movement of the two domains, we shortened the 11-residue linker by either one residue (ΔQ60) or by five residues (F61-RFE-P65). Unfortunately, we were unable to purify any of the ΔFRFEP NfnABC mutant using affinity chromatography with the affinity (His-) tag at the N terminus of NfnC, suggesting that the linker and associated domain flexibility are essential for holoenzyme assembly. In contrast, the single-deletion ΔQ60 mutant was successfully purified, similar to the wild-type enzyme (Fig. S17). Surprisingly, deletion of the Gln residue resulted in a 70% reduction in bifurcating activity, while the artificial dye benzyl viologen (BV)-linked NADPH oxidation activity remained unaffected (Table 1). Clearly, the nature of the linker is critical for relative movement of the two NfnC terminal domains, although as expected, this has no impact on the efficiency of NADPH oxidation by the remote FAD in the NfnA subunit, where BV interactions are unknown but likely do not involve NfnC.

Herein, we proposed that during electron bifurcation of the low potential electron on the C1 cluster of NfnC is transferred to the B3 and then B4 clusters of NfnB, and that it might be possible for Fd to be reduced by the B3 cluster or directly by C1. To explore how essential the B4 cluster was we disrupted it by mutating all four of the Cys that coordinate it. As shown in Figure 3*A* and Fig. S18*C*, from the structural arrangement of the two clusters it might be anticipated that the B3 cluster would still form and be stable in the absence of B4 (given the high cluster content of NfnABC, neither Fe analysis nor electron paramagnetic resonance spectroscopy would distinguish the absence of either just B4 or of B3 and B4). In any event, the NfnB 4C/4A mutant had extremely low bifurcating activity but, as expected given the remoteness of the B3/B4 clusters from the FAD in NfnA, BV-linked NADPH oxidation activity was about 80% of the WT (Table 1). This indicates that a functional B4 and likely B3 are intimately involved in the bifurcation reaction and that the C1 cluster cannot reduce Fd directly.

Discussion

It is remarkable that nature has evolved two kinds of enzymes, NfnSL and NfnABC, with distinct reaction mechanisms to perform the identical physiological function of catalyzing the production NADPH for biosynthesis using NADH and Fd as the electron donors (Equation 1). The first kind belongs to the NfnSL family of enzymes that are simpler and structurally more stable, and their reaction mechanism is well understood, thanks to pioneering structural and mechanistic studies (13, 14). Importantly, the mechanism of NfnSL does not require any significant conformational changes of protein structure. In contrast, the second kind of enzyme is the NfnABC complex that belongs to the much larger and more diverse BfuABC family. The specific activity of Tsi NfnABC is not as high as in the Pfu NfnSL enzyme, which catalyzes the same reaction. However, that of the Tsi enzyme is comparable to the specific activities of other Bfu enzymes, such as Sov Nfn-Bfu (20), Tma FeFe-Bfu (19), and Awo FeFe-Bfu (15), and Amo NiFe-Bfu (16). Indeed, the cellular concentrations of the Bfu enzymes in their native hosts are typically higher than expected, presumably to compensate for these relatively low specific activities.

Why members of the Bfu family all use an FMN, rather than the FAD used in the other three families of electron bifurcating enzymes, is not at all clear. In any event, the electron bifurcation mechanism of the BfuABC family is not understood in general, despite several recent studies (15–17, 20). This has been hampered by definition of the bifurcation site, which cannot be a simple flavin as represented by the BF-FAD in NfnSL, and by the absence of experimental evidence for the site of Fd binding. These issues now resolved with the Tsi NfnABC structures.The significant advances made by this work is that we now know the bifurcation site, a flavobicluster consisting of FMN, a [2Fe-2S] cluster (C1) and a [4Fe-4S] cluster (B1), and we now know where Fd binds. With the new insights provided by Tsi Nfn in hand, future spectroscopic studies can focus on identifying potential intermediate states, such as with added NADPH with and without added Fd and NAD^+. Such an approach can be coupled with a comprehensive structure-guided site-directed mutagenesis effort, along the lines of that carried out herein. Such studies will hopefully provide more insight into the conformation-change coupled reaction mechanism and for the mutants of Tsi NfnABC such analyses are in progress. The structural studies reported here provide the framework for interpreting such results, in order to eventually establish a robust and testable mechanism.

Although the bacterial homolog of Tsi NfnABC found in the bacterial acetogen *S. ovata* assembles a dimer-of-dimers super tetramer with a D2 symmetry (20), we have shown here that the archaeal Tsi Nfn-BfuABC is monomeric and that the monomer is functional. Structural comparison of the monomeric Tsi Nfn-BfuABC with the tetrameric Sov Nfn-BfuABC reveals the former structure lack the long α-helix and the α-helix bundle in the NuoG/Fdh-like domain, which prevent it from forming strong interactions with the NfnL-like domain of other NfnA protomers. Therefore, our work supports the previous conclusion that the bacterial NfnABC is the minimal functional unit, despite its tetrameric super complex assembly. The structure of the Tsi NfnABC is stable in the resting state in the absence of any substrate. However, the electron acceptors NADH and Fd destabilize the NfnBC core, leading to the release of the NfnB Fd-like domain and NfnC CTD from the rigid core to become flexible. Such flexibility has likely enabled the recruitment of the Fd, as we have indeed captured a low-resolution pose of the Tsi NfnABC in which Fd is docked onto the NfnBC core. To our knowledge, this is the first time the electron acceptor Fd has been captured interacting with an electron bifurcating enzyme complex. The conformational dynamics of the NfnBC core and the three conformers we obtained allow us to derive a putative electron bifurcation model. We propose the NAD^+ binding may modulate the flavobicluster switches between the exergonic NAD^+ reduction and endergonic Fd reduction. We suggest the conformational dynamics of the NfnBC core establish a kinetic gate that connect the flavobicluster with the B3/B4 clusters for Fd reduction and further prevent electron backflow from the Fd reduction branch toward the flavobicluster.

In summary, our cryo-EM structural analysis of Tsi NfnABC has revealed the overall architecture, the general conservation, and unique features of the first archaeal BfuABC enzyme, and the acceptor-binding associated conformational changes and the reconfiguration of the electron transfer paths that are likely relevant to electron transfer during bifurcation process. Our work adds to the expanding knowledge of this diverse and somewhat mysterious BfuABC family of enzymes, which includes NiFe- and FeFe-based hydrogenases. They all couple the NAD- and Fd-dependent bifurcation reaction within a highly conserved BfuBC module to a variety of third reactions. The Bfu family is a paradigm of modular evolution in anaerobic metabolism that adapts to a variety of extreme metabolic conditions. Herein we establish a framework of electron transfer pathways and redox-linked conformational changes that are a hallmark of the Bfu family and can be used for

spectroscopic probing of all members of that family to eventually elucidate their common mechanism of action.

Experimental procedures

Expression, purification, and characterization of T. sibiricus *NfnABC*

The Tsi NfnABC operon was expressed in the archaeon *P. furiosus* and the His-tagged recombinant enzyme was purified anaerobically *via* affinity and anion exchange chromatography steps (17). Elemental analysis was performed by Inductively Coupled Plasma Mass Spectrometry (ICP-MS) as previously described (18). Electron bifurcating activity was measured in the bifurcating direction (forward reaction of Equation 1) by following reduction of *P. furiosus* Fd at 425 nm (ϵ = 13 mM^{-1} cm^{-1}) at 80 °C. The reaction mixture contained 0.5 mM NADPH, 2 μM FMN, 1 mM NAD^+, and 25 μM Pfu Fd. FMN was added to replace any that may have dissociated and lost during purification.

Site-directed mutagenesis of T. sibiricus *NfnABC*

WT Tsi NfnABC previously expressed in *P. furiosus* strain MW668 (17) on the plasmid pDN059 was used as the starting point for construction of the NfnA K165E (A7 cluster), the NfnB 4C/4A (B4 cluster) and the NfnC ΔQ and ΔFRFEP (linker) mutants. For the NfnA and NfnC mutations, two rounds of PCR were performed to introduce mutations using the primers listed in Table S1. The first round of PCR contained two reactions and used pDN059 as the template, where fragment one was obtained from the reaction using primer pair P1 and P5 (Table S1), and fragment two was obtained from the reaction using primer pair P2 and P4. The second round of PCR had one reaction producing fragment three using fragment one as the template and P3 and P5 as primers. Primer P3 contained the mutated base pairs. For subsequent Gibson assembly (New England Biolabs), there was a >20 bp overlap between P4 and P5 as well as between P2 and P3. Finally, fragments two and three were ligated into a plasmid by Gibson assembly. By this procedure, pSW006 was made for the NfnA K165E mutant, pSW008 was made for the NfnC ΔQ (linker) mutant, and pSW011 was made for the NfnC ΔFRFEP (linker) mutant. For the NfnB 4C/4A (B4 cluster) mutant, a 500-bp fragment containing the mutations (four Cys changed to four Ala) was synthesized (Twist Bioscience) and the fragment containing the rest of pDN059 was amplified with pDN059 as the template with SW042 and SW043 as primers. Subsequently, the two fragments were ligated by Gibson assembly to produce pSW012. After sequence verification, the four plasmids were linearized by digestion with XhoI, and then transformed into *P. furiosus* COM1 strain as previously described (17).

The growth of the recombinant strains and mutant enzyme purification were performed as previously described (17) but with the following modifications. The strains were grown in 5 L YM5 medium supplemented with 0.05 μg/ml riboflavin and 38 μM ferrous ammonium sulfate at 85 °C for 5 h then at 75 °C for 30 h with shaking at 120 rpm. The cells were harvested by centrifugation at 10,000*g* for 15 min at 10 °C and stored at −20 °C. The cells were lysed by sonication, and cytoplasmic extracts were obtained by centrifugation at 140,000*g* at 4 °C for 1 h. The mutant proteins were purified anaerobically using an NGC Chromatography System (Bio-Rad) with a 5-ml HisTrap Crude column (Cytiva) and then a 5-ml HiTrap Q HP column (Cytiva). Purity was ascertained by SDS-PAGE with a 4 to 15% gradient. Enzyme activities were measured as previously described (17).

Cryo-EM grid preparation and data collection

All NfnABC samples prepared for EM analysis were supplemented with 20 μM FMN to compensate for potential losses during purification. The NAD(H)/Fd-bound samples were prepared by adding NADH (50 μM) and oxidized *P. furiosus* ferredoxin (∼10 μM) to the enzyme (2 mg/ml) and storing the mixture at −80 °C before applying it to cryo-EM grids. To minimize sample exposure to air, 4 μl of each sample was promptly applied to a holey carbon grid (Quantifoil Cu R1.2/1.3, 300 mesh) that were freshly glow-discharged for 30 s. The EM grids were immediately blotted using a piece of Whatman 595 filter paper with the blot force set to three and blot time set to 3 s, without a waiting period. The blotted EM grids were immediately flash-frozen in liquid ethane using FEI Vitrobot Mark IV with the chamber temperature set to 10 °C and the relative humidity set to 100%. Cryo-EM images were collected in a FEI Titan Krios electron microscope (Thermo Fisher Scientific, operated at 300 kV) equipped with a Gatan K3 summit direct detector and a GIF quantum energy filter. Data acquisition was performed with SerialEM (29) in the superresolution mode at a magnification of 105,000 and a pixel size of 0.414 Å at specimen level. The objective lens defocus value was varied from −1.0 to −1.8 μm. During 1.5-s exposure, 50 frames (0.03 s per frame and the dose of 1.2 e/frame/$Å^2$) were collected for each micrograph with a total dose of 60 electrons per $Å^2$.

Image processing and 3D construction

We collected 20,798 raw movie micrographs for Tsi NfnABC holoenzyme and 18,072 raw movie micrographs for the NAD(H)/Fd-bound Tsi NfnABC. All the micrographs were binned by a factor of two and drift corrected with electron-dose weighting in MotionCor 2.1 (30). Contrast Transfer Function (CTF) parameters of each aligned micrograph were estimated and the CTF effect was corrected using CTFFIND 4.1 (31). We used template picking to generate an initial dataset of 12,889,202 particles for the holoenzyme and 11,607,650 particles for the NAD(H)/Fd-bound Tsi NfnABC and performed 2D classification. Good 2D classes containing NfnABC complex were selected, and a few selected averages were used to train Topaz (32), and the following Topaz particle picking yielded 2,053,869 particles for the holoenzyme and 1,221,374 particles for NAD(H)/Fd-bound NfnABC. After 2D classification of this dataset, good 2D classes from template-based picking and the Topaz picking were combined, and duplicated particles were removed. A total of 798,042 particles for the holoenzyme and 1,355,006 particles for the NAD(H)/

Fd-bound Tsi NfnABC were subjected for *ab initio* 3D reconstruction in CryoSPARC (version 4) (33), followed by heterogeneous refinement to generate five EM maps. The best map with good quality of NfnABC contained a total of 342,791 particle images for the holoenzyme and 705,603 particles images for the NAD(H)/Fd-enzyme. The good particle stacks from CryoSPARC were exported to the RELION format by UCSF pyem (https://github.com/asarnow/pyem). One round of 3D classification was performed. Good 3D classes containing a total of 198,898 particle images for the holoenzyme and 458,032 particles images for NAD(H)/Fd-bound NfnABC were selected for further 3D refinement, postprocessing, CTFrefinement, and Bayesian polishing. The final EM map reached an overall resolution of 2.85 Å for the holoenzyme and 2.76 Å for the NAD(H)/Fd-bound form as estimated by the gold-standard Fourier shell correlation at a correlation cutoff value of 0.143 (Figs. S1 and S2). The local resolution map was calculated using ResMap (34). We used EMReady to improve the visual presentation of the final map (35).

Model building, refinement, and validation

We modeled the EM map of the Tsi NfnABC holoenzyme by using the AlphaFold2 (36) predicted structures of the Tsi NfnA, B, C structures. The predicted Tsi NfnA, B, and C models were docked as individual rigid bodies into the high-resolution EM map, respectively. The subunits were merged and subjected to manual building and adjustment in COOT (37), followed by real-space refinement in PHENIX (38). The refined structure was used as the initial model for modeling the EM density map of NAD(H)/Fd-bound NfnABC. Manual model building was performed in COOT (37), followed by real-space refinement in PHENIX (38). The final models were validated using MolProbity (39, 40). Structural figures were generated in UCSF Chimera (41) and ChimeraX (42). Cryo-EM data collection, refinement, and validation statistics are listed in Table S1.

Protein dynamics analysis

The 3DVA (28) in CryoSPARC (version 4) (33) was used to analyze the conformational change observed in the dataset of NAD(H)/Fd-bound Tsi NfnABC. Filter resolution was set to 4 Å before running the program. Twenty clusters (density maps) were generated, and low pass filtered to 8 Å from 3DVA display. The density maps show the movement of NfnC CTD and show the presence of Fd domain. The structural model of the NfnC CTD from NfnABC and Fd domain from Protein Data Bank ID 3SIZ were rigid-body docked into each density map in ChimeraX. Manual adjustments of the NfnC CTD and Fd were performed in COOT (37), followed by real-space refinement in PHENIX (38). Figures and movies were generated in UCSF Chimera (41) and ChimeraX (42).

In silico analysis

For each tree, the sequences were retrieved with DELTA-BLAST to search for conserved domains. The protein BLAST (BLASTp) parameter values used are identity cutoff of >30%, coverage cutoff of >75%, *e*-value cutoff of 10^{-3}. Five hundred sequences were selected and multialigned with MUSCLE and trimmed with trimAl. The ML tree was constructed with the software iq-tree, which chooses the best-fit substitution model. The trees were rooted midpoint, assuming constant evolutionary rate.

Data availability

Cryo-EM 3D map of the Tsi NfnABC holoenzyme at 2.85 Å average resolution and NAD(H)/Fd-bound Tsi NfnABC at 2.76 Å average resolution have been deposited in the Electron Microscopy Data Bank under accession codes EMDB-49039 and EMDB-49040. The corresponding atomic model have been deposited in the Protein Data Bank under accession code 9N5U for the holoenzyme and 9N5V for the NAD(H)/Fd-bound enzyme.

Supporting information—This article contains supporting information.

Acknowledgments—Cryo-EM data were collected at the David Van Andel Advanced Cryo-Electron Microscopy Suite at Van Andel Institute (VAI). We thank Gongpu Zhao and Xing Meng for help with EM data collection, and Daniel Bautista from Bioinformatics and Biostatistics Core for in silico phylogenetic analysis.

Author contributions—X. X., G. J. S., X. F., D. M. N. N., H. H., S. W., and H. L. formal analysis; X. X., G. J. S., X. F., D. M. N. N., H. H., and S. W., investigation; X. X., G. J. S., X. F., D. M. N. N., H. H., and S. W. data curation; X. X., G. J. S., and X. F. validation; X. X., G. J. S., and X. F., visualization; X. X., H. L., and M. W. W. A. methodology; X. X., H. L., and M. W. W. A. conceptualization; X. X. writing–original draft; G. J. S., X. F., D. M. N. N., H. H., H. L., and M. W. W. A. writing–review and editing; H. L. and M. W. W. A. supervision; H. L. and M. W. W. A. funding acquisition.

Funding and additional information—This work was funded by grants from the Division of Chemical Sciences, Geosciences and Biosciences, Office of Basic Energy Sciences of the U.S. Department of Energy (DE-SC0020085 to H.L. and DE-FG02–95ER20175 to M. W. W. A.) and the Van Andel Institute (H. L.).

Conflict of interest—The authors declare that they have no conflicts of interest with the contents of this article.

Abbreviations—The abbreviations used are: 3DVA, 3D variability analysis; BF, bifurcation; BV, benzyl viologen; CTD, C-terminal domain; CTF, contrast transfer function; EB, electron bifurcation; NTD, N-terminal domain.

References

1. Buckel, W., and Thauer, R. K. (2018) Flavin-based electron bifurcation, A new mechanism of biological energy coupling. *Chem. Rev.* **118**, 3862–3886
2. Buckel, W., and Thauer, R. K. (2018) Flavin-based electron bifurcation, ferredoxin, flavodoxin, and anaerobic respiration with protons (Ech) or NAD^+ (Rnf) as electron acceptors: a historical review. *Front. Microbiol.* **9**, 401
3. Buckel, W. (2021) Energy conservation in fermentations of anaerobic bacteria. *Front. Microbiol.* **12**, 703525

4. Mitchell, P. (1975) The protonmotive Q cycle: a general formulation. *FEBS Lett.* **59**, 137–139
5. Peters, J. W., Miller, A.-F., Jones, A. K., King, P. W., and Adams, M. W. W. (2016) Electron bifurcation. *Curr. Opin. Chem. Biol.* **31**, 146–152
6. Herrmann, G., Jayamani, E., Mai, G., and Buckel, W. (2008) Energy conservation via electron-transferring flavoprotein in anaerobic bacteria. *J. Bacteriol.* **190**, 784–791
7. Li, F., Hinderberger, J., Seedorf, H., Zhang, J., Buckel, W., and Thauer, R. K. (2008) Coupled ferredoxin and crotonyl coenzyme A (CoA) reduction with NADH catalyzed by the butyryl-CoA dehydrogenase/Etf complex from *Clostridium kluyveri*. *J. Bacteriol.* **190**, 843–850
8. Schut, G. J., and Adams, M. W. W. (2009) The iron-hydrogenase of *Thermotoga maritima* utilizes ferredoxin and NADH synergistically: a new perspective on anaerobic hydrogen production. *J. Bacteriol.* **191**, 4451–4457
9. Buckel, W., and Thauer, R. K. (2013) Energy conservation via electron bifurcating ferredoxin reduction and proton/Na^+ translocating ferredoxin oxidation. *Biochim. Biophys. Acta (BBA) - Bioenerg.* **1827**, 94–113
10. Bertsch, J., Parthasarathy, A., Buckel, W., and Müller, V. (2013) An electron-bifurcating caffeyl-CoA reductase. *J. Biol. Chem.* **288**, 11304–11311
11. Demmer, J. K., Bertsch, J., Öppinger, C., Wohlers, H., Kayastha, K., Demmer, U., *et al.* (2018) Molecular basis of the flavin-based electron-bifurcating caffeyl-CoA reductase reaction. *FEBS Lett.* **592**, 332–342
12. Feng, X., Schut, G. J., Lipscomb, G. L., Li, H., and Adams, M. W. W. (2021) Cryoelectron microscopy structure and mechanism of the membrane-associated electron-bifurcating flavoprotein Fix/EtfABCX. *Proc. Natl. Acad. Sci.* **118**, e2016978118
13. Demmer, J. K., Huang, H., Wang, S., Demmer, U., Thauer, R. K., and Ermler, U. (2015) Insights into flavin-based electron bifurcation via the NADH-dependent reduced ferredoxin:NADP oxidoreductase structure. *J. Biol. Chem.* **290**, 21985–21995
14. Lubner, C. E., Jennings, D. P., Mulder, D. W., Schut, G. J., Zadvornyy, O. A., Hoben, J. P., *et al.* (2017) Mechanistic insights into energy conservation by flavin-based electron bifurcation. *Nat. Chem. Biol.* **13**, 655–659
15. Katsyv, A., Kumar, A., Saura, P., Pöverlein, M. C., Freibert, S. A., T Stripp, S., *et al.* (2023) Molecular basis of the electron bifurcation mechanism in the [FeFe]-Hydrogenase complex HydABC. *J. Am. Chem. Soc.* **145**, 5696–5709
16. Feng, X., Schut, G. J., Haja, D. K., Adams, M. W. W., and Li, H. (2022) Structure and electron transfer pathways of an electron-bifurcating NiFe-hydrogenase. *Sci. Adv.* **8**, eabm7546
17. Schut, G. J., Haja, D. K., Feng, X., Poole, F. L., Li, H., and Adams, M. W. W. (2022) An abundant and diverse new family of electron bifurcating enzymes with a non-canonical catalytic mechanism. *Front. Microbiol.* **13**, 946711
18. Schut, G. J., Thorgersen, M. P., Poole, F. L., 2nd, Haja, D. K., Putumbaka, S., and Adams, M. W. W. (2021) Tungsten enzymes play a role in detoxifying food and antimicrobial aldehydes in the human gut microbiome. *Proc. Natl. Acad. Sci.* **118**, e2109008118
19. Furlan, C., Chongdar, N., Gupta, P., Lubitz, W., Ogata, H., Blaza, J. N., *et al.* (2022) Structural insight on the mechanism of an electron-bifurcating [FeFe] hydrogenase. *eLife* **11**, e79361
20. Kumar, A., Kremp, F., Roth, J., Freibert, S. A., Müller, V., and Schuller, J. M. (2023) Molecular architecture and electron transfer pathway of the Stn family transhydrogenase. *Nat. Commun.* **14**, 5484
21. Nguyen, D. M. N., Schut, G. J., Zadvornyy, O. A., Tokmina-Lukaszewska, M., Poudel, S., Lipscomb, G. L., *et al.* (2017) Two functionally distinct $NADP^+$-dependent ferredoxin oxidoreductases maintain the primary redox balance of *Pyrococcus furiosus*. *J. Biol. Chem.* **292**, 14603–14616
22. Kremp, F., Roth, J., and Müller, V. (2020) The Sporomusa type Nfn is a novel type of electron-bifurcating transhydrogenase that links the redox pools in acetogenic bacteria. *Scientific Rep.* **10**, 14872
23. Gutiérrez-Fernández, J., Kaszuba, K., Minhas, G. S., Baradaran, R., Tambalo, M., Gallagher, D. T., *et al.* (2020) Key role of quinone in the mechanism of respiratory complex I. *Nat. Commun.* **11**, 4135
24. Young, T., Niks, D., Hakopian, S., Tam, T. K., Yu, X., Hille, R., *et al.* (2020) Crystallographic and kinetic analyses of the FdsBG subcomplex of the cytosolic formate dehydrogenase FdsABG from *Cupriavidus necator*. *J. Biol. Chem.* **295**, 6570–6585
25. Zuchan, K., Baymann, F., Baffert, C., Brugna, M., and Nitschke, W. (2021) The dyad of the Y-junction- and a flavin module unites diverse redox enzymes. *Biochim. Biophys. Acta (BBA) - Bioenerg.* **1862**, 148401
26. Hinchliffe, P., and Sazanov, L. A. (2005) Organization of iron-sulfur clusters in respiratory complex I. *Science* **309**, 771–774
27. Chánique, A. M., and Parra, L. P. (2018) Protein engineering for nicotinamide coenzyme specificity in oxidoreductases: attempts and challenges. *Front. Microbiol.* **9**, 194
28. Punjani, A., and Fleet, D. J. (2021) 3D variability analysis: resolving continuous flexibility and discrete heterogeneity from single particle cryo-EM. *J. Struct. Biol.* **213**, 107702
29. Mastronarde, D. N. (2003) SerialEM: a program for automated tilt series acquisition on Tecnai microscopes using prediction of specimen position. *Microsc. Microanalysis* **9**, 1182–1183
30. Zheng, S. Q., Palovcak, E., Armache, J. P., Verba, K. A., Cheng, Y., and Agard, D. A. (2017) MotionCor2: anisotropic correction of beam-induced motion for improved cryo-electron microscopy. *Nat. Methods* **14**, 331–332
31. Rohou, A., and Grigorieff, N. (2015) CTFFIND4: fast and accurate defocus estimation from electron micrographs. *J. Struct. Biol.* **192**, 216–221
32. Bepler, T., Morin, A., Rapp, M., Brasch, J., Shapiro, L., Noble, A. J., *et al.* (2019) Positive-unlabeled convolutional neural networks for particle picking in cryo-electron micrographs. *Nat. Methods* **16**, 1153–1160
33. Punjani, A., Rubinstein, J. L., Fleet, D. J., and Brubaker, M. A. (2017) cryoSPARC: algorithms for rapid unsupervised cryo-EM structure determination. *Nat. Methods* **14**, 290–296
34. Kucukelbir, A., Sigworth, F. J., and Tagare, H. D. (2014) Quantifying the local resolution of cryo-EM density maps. *Nat. Methods* **11**, 63–65
35. He, J., Li, T., and Huang, S.-Y. (2023) Improvement of cryo-EM maps by simultaneous local and non-local deep learning. *Nat. Commun.* **14**, 3217
36. Jumper, J., Evans, R., Pritzel, A., Green, T., Figurnov, M., Ronneberger, O., *et al.* (2021) Highly accurate protein structure prediction with AlphaFold. *Nature* **596**, 583–589
37. Emsley, P., Lohkamp, B., Scott, W. G., and Cowtan, K. (2010) Features and development of coot. *Acta Crystallogr. D Biol. Crystallogr.* **66**, 486–501
38. Adams, P. D., Afonine, P. V., Bunkóczi, G., Chen, V. B., Davis, I. W., Echols, N., *et al.* (2010) PHENIX: a comprehensive Python-based system for macromolecular structure solution. *Acta Crystallogr. D Biol. Crystallogr.* **66**, 213–221
39. Chen, V. B., Arendall, W. B., Headd, J. J., Keedy, D. A., Immormino, R. M., Kapral, G. J., *et al.* (2010) MolProbity: all-atom structure validation for macromolecular crystallography. *Acta Crystallogr. D Biol. Crystallogr.* **66**, 12–21
40. Williams, C. J., Headd, J. J., Moriarty, N. W., Prisant, M. G., Videau, L. L., Deis, L. N., *et al.* (2018) MolProbity: more and better reference data for improved all-atom structure validation. *Protein Sci.* **27**, 293–315
41. Pettersen, E. F., Goddard, T. D., Huang, C. C., Couch, G. S., Greenblatt, D. M., Meng, E. C., *et al.* (2004) UCSF Chimera—a visualization system for exploratory research and analysis. *J. Comput. Chem.* **25**, 1605–1612
42. Goddard, T. D., Huang, C. C., Meng, E. C., Pettersen, E. F., Couch, G. S., Morris, J. H., *et al.* (2018) UCSF ChimeraX: meeting modern challenges in visualization and analysis. *Protein Sci.* **27**, 14–25